Electrochemistry Communications 91 (2018) 41–44

Contents lists available at ScienceDirect

Electrochemistry Communications

journal homepage: www.elsevier.com/locate/elecom

# The missing piece of the puzzle regarding the relation between the degree of superhydrophobicity and the corrosion resistance of superhydrophobic coatings

A. Bahgat Radwan, Aboubakr M. Abdullah*, Mohammad K. Hassan

*Center for Advanced Materials, Qatar University, Doha, P.O. Box 2713, Qatar*

ARTICLE INFO

*Keywords:*
Superhydrophobic
Nanocomposite
Coatings
Corrosion
Dielectric properties

ABSTRACT

This work supplies the missing piece of the puzzle regarding the unclear relation between the water contact angle (WCA) of a superhydrophobic coating (SHC) and its corrosion protection performance. Generally, an increase in the WCA of a coating increases its corrosion protection behavior. However, in some cases it has been reported that an increase in the WCA, inexplicably, reduces its corrosion protection efficiency. This work uses measurements of the dielectric properties of a SHC to reveal the main reason behind a significant increase in the corrosion protection efficiency of a SHC when there are minor or no changes in the values of the measured WCA.

## 1. Introduction

A surface is called superhydrophobic when it exhibits a water contact angle (WCA) ≥ 150° and a low water sliding angle (WSA) (and thereby a low water contact angle hysteresis, WCAH) [1–3]. Two models relate the surface superhydrophobicity (SSH) to its roughness. The Wenzel model summarizes this relation by Eq. (1):

$$\cos\theta^* = r\cos\theta \quad (1)$$

where $\theta^*$ is the apparent static contact angle, $\theta$ is the static contact angle of an ideal smooth surface and $r$ is the ratio between the actual surface area and the geometrical one [2].

By contrast, the Cassie–Baxter model attributes the SSH to the air trapped within the pockets underneath a liquid droplet which prevents it from penetrating the surface [4]. Tremendous efforts have therefore focused on controlling the superhydrophobicity of different surfaces of metals and their coatings to enhance their corrosion resistance properties [5–12]. Generally, it has been found that the higher the WCA of a superhydrophobic coating (SHC), the better its corrosion resistance [4–12]. However, Nine et al. noticed exactly the opposite. They prepared three different polydimethylsiloxane (PDMS)-based SHCs on Cu substrates with a WCA greater than 150° [13], but the coating with the lowest WCA (154° ± 1) had a higher corrosion protection efficiency than the other SHCs, which had WCAs of 159° ± 1 and 170° ± 2. A similar observation was also reported by Wang et al. [14].

The goal of this work is to reveal the reason behind the discrepancies in the corrosion protection properties of some SHCs of the same base material despite their high WCAs. To achieve this two different SHCs, one composed of pure poly(vinylidene-*co*-hexafluoropropylene) (PVDFHFP) and the other of a PVDFHFP nanocomposite with 0.5% $Al_2O_3$ nanoparticles, were synthesized on Al, and their corrosion protection performance and dielectric properties were measured.

## 2. Experimental

Two porous SHCs (same pore size) were fabricated on mirror-like polished Al surfaces using the electrospinning technique (flow rate 1.5 mL $h^{-1}$; distance = 15 cm; applied potential 20 kV; dimethyl formamide solvent, BDH, England): (i) PVDFHFP (400,000 g $mol^{-1}$, Sigma-Aldrich, Munich, Germany) and (ii) a PVDFHFP–$Al_2O_3$ nanocomposite ($Al_2O_3$ nanoparticle < 20 nm, Sigma-Aldrich, Munich, Germany). The preparation procedure was as follows: 3.75 g of PVDFHFP was dissolved in 50 mL of DMF (Sigma-Aldrich, Munich, Germany) at 35 °C for 12 h under vigorous stirring (600 rpm) to obtain a homogeneous solution. 0.15 g of $Al_2O_3$ nanoparticles were separately dispersed in 25 mL of DMF, and then the $Al_2O_3$ dispersion was added to the PVDFHFP solution. The PVDFHFP–$Al_2O_3$ solution was then electrospun using a TONGLI TL Electrospinning & Spray Unit (NEU-01) (Nanshan, Shenzhen, China). A needle with an inside diameter of 0.25 mm was used and the operating temperature was kept constant at 35 °C. High field emission scanning electron microscopy, HFESEM, (FEI NOVA NANOSEM 450, Hillsboro, OR, USA) was used to document the morphology. In addition, the WCA was measured using Dataphysics

* Corresponding author.
*E-mail address:* bakr@qu.edu.qa (A.M. Abdullah).

https://doi.org/10.1016/j.elecom.2018.05.008
Received 7 March 2018; Received in revised form 4 May 2018; Accepted 4 May 2018
Available online 05 May 2018
1388-2481/ 

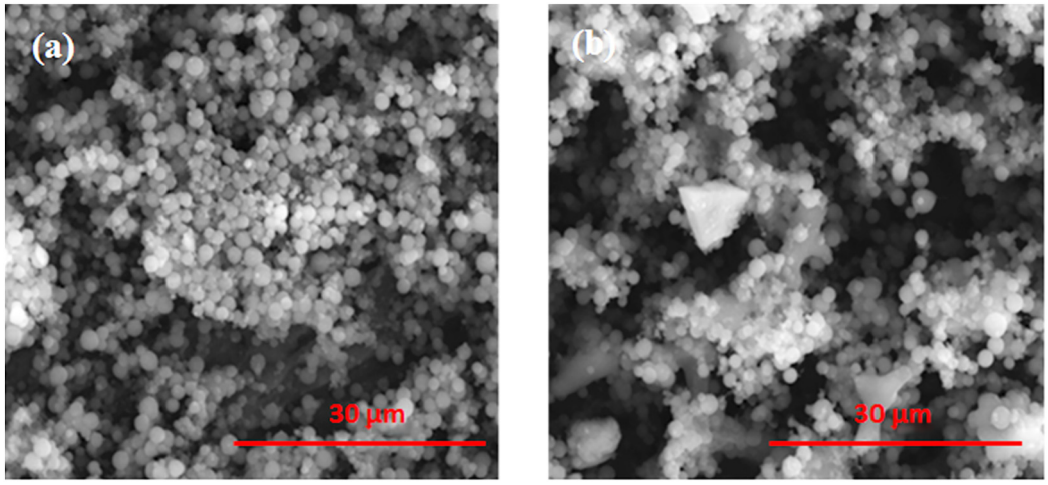


**Fig. 1.** SEM micrographs of (a) pure PVDFHFP and (b) PVDFHFP–$Al_2O_3$ SHCs.

OCA 35 (Filderstadt, Germany). The corrosion performance of the Al/PVDFHFP and the AL/PVDFHFP–$Al_2O_3$ coatings was estimated using electrochemical impedance spectroscopy (EIS) in 3.5% NaCl solution using a Reference 3000 potentiostat (Gamry, Warminster, PA, USA) between $1 \times 10^5$ and $1 \times 10^{-2}$ Hz. Finally, the dielectric measurements were performed using the parallel plate capacitor technique in which a film of the polymer is sandwiched between the parallel plates of a capacitor. A Novocontrol GmbH Concept 40 broadband dielectric spectrometer (Novocontrol Technologies, Montabaur, Germany) was used, and data were collected over the frequency (f) range 0.1–3 M Hz at 20 °C. The AC conductivity is calculated using Novocontrol WinDETA software, by using the measured values of dielectric permittivity storage (ε′) and the dielectric loss factor (ε″).

## 3. Results and discussion

Fig. 1 shows SEM micrographs that reveal the morphology of the PVDFHFP and PVDFHFP–$Al_2O_3$ coatings. Both show beaded fibers which are attributed to insufficiently fast stretching during the flagellation of the jet [15]. This combination of the microscale structure of the beads and the nano-scale of the fibers leads to an increase in the WCA to 150° ± 3 and 152° ± 2 with CAH (contact angle hysteresis) values of 4° ± 2 and 3.5° ± 1 for PVDFHFP and PVDFHFP–$Al_2O_3$ coatings, respectively. It is worth noting that the surface roughness values of the PVDFHFP and PVDFHFP–$Al_2O_3$ SHCs are 60 and 86 nm, respectively.

The impedance parameters listed in Table 1 are derived from the measured EIS data (symbols) shown in Fig. 2 after fitting them (solid lines) using the equivalent circuits shown in the insets of the same figure.

In the equivalent circuits, $R_s$ is constant for 3.5% NaCl solutions and is equal to ~5 Ω. $R_{po}$ represents the pore resistance of a coating. $R_{ct1}$ and $R_{ct2}$ are charge-transfer resistances. $W$ is the Warburg diffusion impedance and CPE1, CPE2 and CPE3 are constant phase elements for non-ideal electrical double layers. The addition of $Al_2O_3$ to the PVDHFP coating markedly increases the charge transfer resistance from 50 to 1000 kΩ·cm$^2$, although the difference in the WCAs for both coatings is negligible. Moreover, the non-ideal double layer capacitances of the SHCs is significantly decreased from $1 \times 10^{-4}$ and $1.2 \times 10^{-5}$ for the PVDFHFP to $2.3 \times 10^{-7}$ and $8.1 \times 10^{-7}$ s$^n$ ohm$^{-1}$ cm$^{-2}$ for the PVDHFP–$Al_2O_3$. The straight line in the low-frequency regions in Fig. 2b and c can be attributed to diffusion across the porous coatings. The Warburg diffusion, $W$, is reduced from $1.2 \times 10^{-4}$ to $8 \times 10^{-6}$ Ω·s$^{-1/2}$ for PVDFHFP and PVDHFP–$Al_2O_3$, respectively. The mechanism proposed in the literature explains the corrosion protection of SHCs in terms of the trapped air within the holes of the rough surface of a SHC preventing hydrated aggressive ions, e.g. $Cl^-$ ions, from attacking the metal surfaces beneath. In the present case, since the WCAs for both SHCs are almost the same, the amount of trapped air should be nearly the same, according to Eq. (2):

$$\cos\theta_{CB} = r_f f_1 \cos\theta_Y - f_2 \quad (2)$$

where $r_f$ is the roughness ratio, $\theta_{CB}$ is the Cassie–Baxter contact angle, and $\theta_Y$ is the "intrinsic" contact angle on a flat surface with the same chemistry. Cassie and Baxter denoted $f_1$ and $f_2$ as the liquid–solid and the liquid–air fractional areas under a droplet, respectively, where $f_1 + f_2 = 1$. This means that the obstructive influence of the trapped air within both coatings should be nearly the same i.e. their corrosion protection efficiencies should be the same according to this mechanism. However, this does not happen. Consequently, the mechanism based on the penetration of aggressive ions reported in the literature cannot explain the current phenomenon. Further characterization was therefore carried out using dielectric spectroscopy in order to explore this behavior.

The dielectric constant (ε′) and the AC conductivity (σ′) of the neat PVDFHFP and PVDFHFP–$Al_2O_3$ nanofiber composite samples are given in Fig. 3. Many features can be deduced from the curves of these plots. At low$f$, time scale or half period of oscillation $(2f)^{-1}$, ε′ increases as $f$ decreases for the neat PVDFHFP sample. Charge carriers and ionic moieties can achieve more hops before the applied field reverses [16].

**Table 1**
EIS spectra-derived parameters for the bare Al substrate, Al/PVDFHFP and Al/PVDFHFP–$Al_2O_3$ in 3.5% NaCl at OCP in a frequency range of $1 \times 10^5$ to $1 \times 10^{-2}$ Hz at 25 °C. All specimens were pre-immersed in the same electrolyte for 30 min before starting the measurements.

| Sample | $R_{po}$ (kΩ·cm$^2$) | $R_{ct}$ (kΩ·cm$^2$) | $W$ (Ω/s$^{1/2}$) | CPE1 (s$^n$ ohm$^{-1}$ cm$^{-2}$) | CPE2 (s$^n$ ohm$^{-1}$ cm$^{-2}$) | CPE3 (s$^n$ ohm$^{-1}$ cm$^{-2}$) | $n1$ | $n2$ |
|---|---|---|---|---|---|---|---|---|
| Al | – | 3 | – | $7.0 \times 10^{-5}$ | – | – | 0.89 | – |
| PVDFHFP | 1 | 50 | $1.2 \times 10^{-4}$ | – | $1.0 \times 10^{-4}$ | $1.2 \times 10^{-5}$ | 0.88 | 0.93 |
| PVDFHFP–$Al_2O_3$ | 120 | 1000 | $8 \times 10^{-6}$ | – | $2.3 \times 10^{-7}$ | $8.1 \times 10^{-7}$ | 0.764 | 0.83 |